Back-contacted high-efficiency silicon solar cells – conversion efficiency dependence on cell thickness

Felix Haase[1], **Sarah Kajari-Schröder**[1], **Renate Winter**[1], **Martin Nese**[2] & **Rolf Brendel**[1,3]
[1]Institute for Solar Energy Research Hamelin (ISFH), Emmerthal, Germany; [2]EPISUN AS, Oslo, Norway;
[3]Institute for Solid State Physics, Leibniz Universität Hannover, Germany

ABSTRACT

Reducing the cost of photovoltaic energy is the main objective of solar cell manufacturers. This is ideally realized by increasing cell efficiency and simultaneously decreasing manufacturing cost. To reduce fabrication costs, the international roadmap of photovoltaics (ITRPV) forecasts a reduction in cell thickness from 180µm to 120µm in the next six years, and even thinner cells may be desirable, as long as efficiency and yield are not negatively affected. In order to increase efficiency, the ITRPV forecasts an increase in share of back-contacted cells from 5% to 35% in the next eight years. In this paper the dependence of the efficiency of back-junction back-contact (BJBC) solar cells on cell thickness is investigated experimentally and numerically. To this end, BJBC silicon solar cells with cell thicknesses ranging from 45µm to 290µm are fabricated and simulated. Thinned float-zone material is used as well as monocrystalline epitaxial layers fabricated by the porous silicon process for 45µm-thick cells. The efficiency of the best cell is 22.6% (130µm cell thickness) and 18.9% for an epitaxial cell (45µm thickness). Loss mechanisms in the maximum power point of all cells are investigated by using a free-energy loss analysis based on finite-element simulations. A lower generation and a lower recombination in thinner cells compete against each other, resulting in a maximum efficiency of 20% for a cell thickness of 45µm at a base lifetime of 20µs. At a base lifetime of 3000µs, the maximum efficiency is greater than 23% for a cell thickness beyond 290µm, but reducing the cell thickness from 290µm to about 90µm results in a power loss of less than 0.6% absolute.

Introduction

Back-junction back-contact (BJBC) silicon solar cells combine a high conversion efficiency potential with a single-side cell interconnection within the module [1,2]. The advantages of the single-side cell interconnection are the reduction of handling steps [3] and the avoidance of micro-cracks by using a conductive foil [4]. By using high-throughput processes, such as ion implantation [5,6] and laser processing [7], the back-junction process may in the future reduce fabrication costs compared to the standard screen-printed solar cell process. Furthermore, the decrease in material consumption also leads to a reduction in costs.

The effect of cell thickness on solar cell efficiency has already been studied for solar cells with two-sided contacts. In 1982 Chih-Tang et al. [8], using low base lifetime material, determined a broad efficiency peak of 17% at around 50µm cell thickness. Kray et al. [9] found that efficiency is practically independent of cell thickness for Czochralski-grown material, and efficiency only slightly increases by up to 1% absolute with increasing cell thickness from 36µm to 250µm for float-zone material. In the latter study, silicon wafers with an initial thickness of 250µm were thinned down by an infeed grinder to achieve the desired thickness. However, for production this technique is obviously not feasible.

> "The highest solar cell conversion efficiency achieved using the latest kerf-less technologies is only 15%, whereas a 19.1% conversion efficiency has been obtained by applying the PSI process."

For this investigation, the porous silicon process (PSI) [10,11], which was first discovered in 1997, is used to fabricate 45µm-thick crystalline silicon films. This technology skips the wafering process, in which 55% of the material is wasted (at a current wafer thickness of 180µm). Alternatives to this technique include the separation of a thin silicon film from a monocrystalline substrate wafer by annealing a stack of metal deposited on top of a silicon wafer and by using ion implantation [12,13].

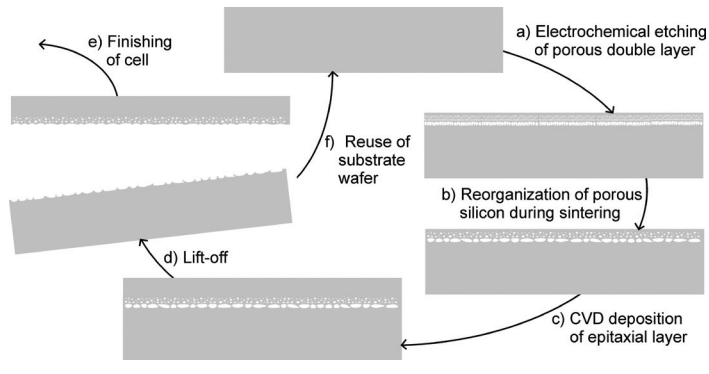

Figure 1. Schematic of the porous silicon process: (a) a porous double layer is electrochemically etched in a substrate wafer – the bottom layer has a high porosity, whereas the upper layer has a low porosity; (b) the porous double layer reorganizes during a sintering step in hydrogen at 1100°C; (c) an epitaxial Si layer grows in a chemical vapour deposition (CVD) at 1100°C; (d) the epitaxial layer is lifted off – the high porosity layer serves as the breaking point; (e) the epitaxial solar cell can be finished; (f) the substrate wafer can be reused for the next PSI cycle.

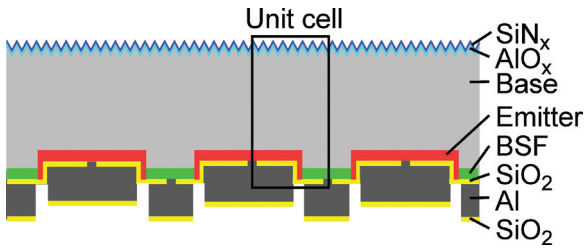

Figure 2. Schematic cross section of the BJBC solar cell (not to scale) – the cross section of the unit cell is indicated by a box. (Adapted from Haase et al. [19].)

However, the highest solar cell conversion efficiency achieved using the latest kerf-less technologies is only 15% [14], whereas a 19.1% conversion efficiency has been obtained by applying the PSI process [15]. To examine the entire thickness range between 45µm and 290µm, thinned float-zone silicon samples are also used.

Fabrication of BJBC solar cells

Float-zone material thinned by wet-chemical etching was used, as well as monocrystalline thin films fabricated by PSI. In this process a porous double layer is etched electrochemically into the surface of a thick silicon wafer, as shown in Fig. 1. After sintering at 1100°C in a hydrogen atmosphere, silicon is grown epitaxially on top of the closed surface of the top porous silicon layer. The growth process controls the layer thickness as well as the doping gradients. Finally, the highly porous bottom layer permits a lifting-off of the epitaxial silicon layer, and a solar cell is then processed from the thin layer. The thick silicon substrate wafer can be reused for many more PSI cycles [16,17]. The material consumption is much lower, since only the porous layer of 2µm is lost in comparison to sawing losses of 120µm.

The cell-thickness dependence of the efficiency will be illustrated by means of BJBC solar cells fabricated with a cell size of 3.92cm^2; all the cells are processed in a single batch for better comparison of the results. A cell process previously developed at ISFH [18] is employed, which uses industrially feasible laser processes and avoids laboratory processes such as photolithography.

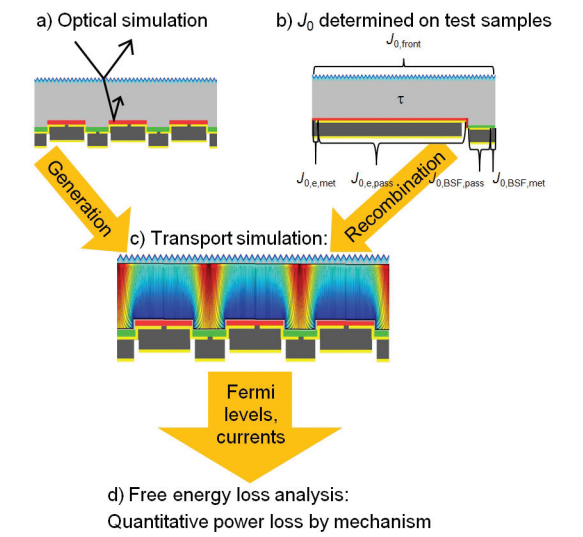

Figure 3. Loss analysis procedure. A simulated generation profile and the saturation current densities determined for test samples are input parameters for the finite-element simulation. Output parameters such as Fermi levels and currents are used for the free-energy loss analysis.

Group	130-1.5	290-1.5		290-0.5		90-0.5		45-0.5	
Cell thickness d [µm]	130	290		290		90		45	
Base resistivity ρ [Ωcm]	1.5	1.5		0.5		0.5		0.5	
Base lifetime τ [µs]	4000	4000		3000		3000		20	
Number of processed cells	1	6		8		12		3	
	best	best	6 best	best	6 best	best	6 best	best	3 best
Open circuit voltage V_{oc} [mV]	671	672	672	673	673	672	669	651*	653
Short circuit current density J_{sc} [mA·cm^{-2}]	41.1	40.9	40.6	39.7	39.2	38.4	37.5	36.0*	35.3
Fill factor FF [%]	81.8	81.9	80.2	81.6	81.3	81.9	80.2	80.6*	79.8
Conversion efficiency η [%]	22.6	22.5	21.9	21.8	21.4	21.1	20.1	18.9*	18.4
$\Delta\eta$ caused by difference in:	cell thickness			cell thickness					
$\Delta\eta$ caused by difference in:		base resistivity and lifetime				base lifetime and cell thickness			

*independently confirmed by Fraunhofer ISE

Table 1. Material properties and parameters of the light *J-V* curves of the five groups investigated in this study. The best cell is shown, as are the average values of the six best cells and of the three best cells.

The cell structure is shown in Fig. 2. The front surface is textured and a 10nm-thick AlO_x passivation layer is deposited by atomic layer deposition. A SiN_x layer serves as an anti-reflection coating. The rear side is processed as an interdigitated finger structure with an index of 1mm. The phosphorous emitter with a sheet resistance of 70Ω/sq covers 84% of the cell rear side. A boron-diffused back-surface field (BSF) with a sheet resistance of 20Ω/sq reduces the recombination rate beneath the contacts. A thermal oxide of thickness 150nm serves as a rear-side passivation and rear reflector. Laser contact opening (LCO) of the passivation layer and subsequent aluminium evaporation form the contacts. This 10µm-thick aluminium layer is etched at the edges separating the emitter and the BSF layer [20].

Five different groups of cells – categorized according to cell thickness and base resistivity – were investigated. Table 1 shows the material properties and parameters of the light *J-V* curves of the processed groups. Cell thicknesses varied from 45µm to 290µm, base resistivities from 1.5Ωcm to 0.5Ωcm and base lifetimes from 20µs to 4000µs.

Loss analysis of BJBC solar cells by means of device simulations

The loss mechanisms in the experimental devices are analyzed by determining the generation, recombination and transport losses. The generation is simulated using the ray tracer SUNRAYS [21]. Input parameters are measured geometries and optical layer properties. To determine the recombination at the surfaces, the Kane-Swanson method [22] is used, which is based on infrared lifetime measurements [23] on test samples that are processed in parallel to the solar cells. The saturation current densities of all passivated and metalized surfaces [24] are determined. The base lifetime is extracted by varying the thickness of these test samples [25].

As shown in Fig. 3 the generation profile from the SUNRAYS simulation (Fig. 3(a)) and the recombination parameters (Fig. 3(b)) are input parameters for a transport simulation (Fig. 3(c)). The transport simulation uses the conductive boundary (CoBo) model [26], which is implemented in the finite-element analyzer COMSOL [27]. The CoBo model treats diffused surfaces as one-dimensional boundaries characterized by a sheet resistance and a saturation current density. A free-energy loss analysis [28] based on the finite-element simulation yields the generated free-energy power densities lost by different mechanisms and extracted as shown in Fig. 3(d).

Fig. 4 shows the simulated power densities at the maximum power point of the five experimentally investigated groups, which are irradiated with an intensity of 1000Wm^{-2}: the generated and both the simulated and measured extracted power densities are plotted. The main power density losses and the sum of all losses are also shown. The extracted power densities of the simulations are about 10Wm^{-2} (corresponding to 1% efficiency points) higher than the measured values. This deviation is attributed to resistive losses at the contacts and in the metal grids (these losses are not implemented in our simulations).

Fig. 5 shows the local minority-carrier current paths; the colour quantifies the power density loss by Shockley-Read-

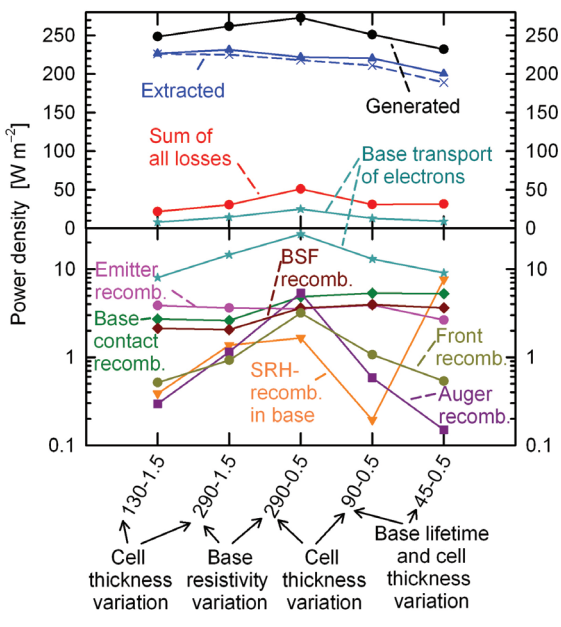

Figure 4. Power densities of unit cells of the five cell groups: simulated generated power densities and both simulated (solid line) and measured (dashed line) extracted power densities are shown. Also indicated are the main power density losses of the unit cells and the sum of these losses. (Adapted from Haase et al. [19].)

Hall (SRH) recombination of the five investigated groups. The minority-carrier current paths start very close to the front surface of the unit cell, and most of them end at the rear surface of the cell. The electrons which follow the paths to the emitter and are not lost by recombination are collected and contribute to the power output. The electrons which follow the other paths are all lost by recombination. The effect of the current paths ending at the rear surface of the base finger is called electrical shading [29]: this area is indicated by a black line on top of the cells.

The simulated impact of cell thickness, base doping and base lifetime on the conversion efficiency and on the local recombination and minority carrier current paths will be discussed next.

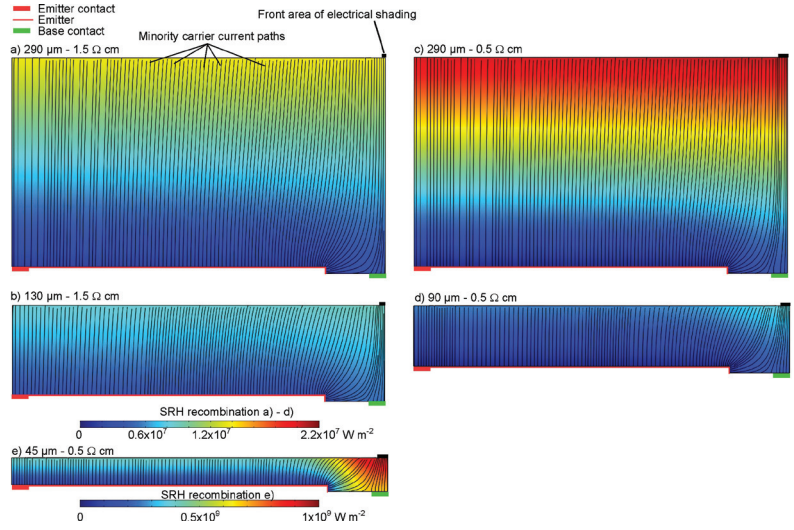

Figure 5. SRH recombination and minority-carrier current paths (black lines) of each unit cell. For comparison purposes the first four cells (a) to (d) are plotted on the same scale, whereas cell 45-0.5 has the highest SRH recombination and therefore uses a wider range. The regions of the contacts, emitter and electrical shading are shown for each cell. (Adapted from Haase et al. [19].)

Impact of cell thickness on conversion efficiency

The thickness dependence is best analyzed by comparing the results of groups 290-0.5 and 90-0.5 or 290-1.5 and 130-1.5, which differ in thickness only, as shown in Table 1. At long wavelengths, the spectral response of thin cells is not as good as thick cells: the generated power density therefore decreases with decreasing cell thickness by 5% relative at a base resistivity of 1.5Ωcm and by 10% relative at a base resistivity of 0.5Ωcm.

The free-energy transport loss of electrons is the highest power density loss for all thickness values, but shows a strong decrease with decreasing cell thickness. The free-energy transport loss of electrons is a quadratic function of the electron quasi-Fermi level gradient. Since this gradient decreases with increasing distance to the emitter, the total electron transport loss F_{bt_e} increases with an exponent x of less than one with increasing distance to the emitter and thus with increasing cell thickness d ($F_{bt\_e} \sim d^x, x<1$).

All power density losses caused by recombination in the base (SRH recombination, Auger recombination) or at the front surface decrease with decreasing cell thickness. The SRH recombination increases with increasing distance to the emitter because of an increase in minority carrier concentration, illustrated by comparing Figs. 5(a) and 5(c) with Figs. 5(b) and 5(d) respectively. The bottom part of cell 290-0.5 shows nearly the same local SRH recombination as cell 90-0.5; a comparison of cell groups 290-1.5 and 130-1.5 indicates the same effect. This characteristic is due to the quasi-Fermi level gradient of the minorities that causes an increase in minority-carrier concentration with increasing distance to the emitter.

On the other hand, the power density losses caused by the rear surface (emitter recombination, BSF recombination and base contact recombination) increase only slightly with decreasing cell thickness. The number of minority-carrier current paths which end in the base contact, where the electrons recombine, slightly increases with decreasing cell thickness. For these two reasons a low recombination at the base finger, and especially at the base contact, becomes more important for thinner cells.

> "Thinner cells benefit from lower front and base recombination, but at the same time suffer from a reduced generation."

In conclusion, thinner cells benefit from lower front and base recombination, but at the same time suffer from a reduced generation. Depending on the specific material properties, a decrease in cell thickness might thus result in either a decrease or an increase in cell efficiency. In the study presented here, decreasing the cell thickness from 290µm to 130µm for 1.5Ωcm and 4000µs material leads to a decrease in conversion efficiency of 0.5% absolute. However, decreasing the cell thickness from 290µm to 90µm for 0.5Ωcm and 3000µs material leads to a decrease in conversion efficiency of only 0.2% absolute.

Impact of base-doping on conversion efficiency

The base-doping dependence is analyzed by comparing the results of groups 290-1.5 and 290-0.5, which differ only in base doping, as shown in Table 1. The base lifetime of both samples does not differ significantly. The power densities are free energies and proportional to the quasi-Fermi level splitting. Decreasing the base resistivity and thus increasing the base-doping density lowers the Fermi level in p-type cells. This leads to an increase in quasi-Fermi level splitting, resulting in an increase in generated power density as well as in power density losses.

The transport loss of electrons is the highest power density loss for both doping densities and increases with increasing base doping. Since the quasi-Fermi level splitting in the base increases but is on the same level at the emitter, the gradient of the electron quasi-Fermi level increases with increasing base doping, which increases the free-energy loss by electron transport.

Auger recombination is proportional to $(n \times p^2)$ at low-level injection in these p-type solar cells. For this reason, Auger recombination increases by a factor of about nine when base doping p increases by a factor of three, which is the case for a decrease in base resistivity from 1.5Ωcm to 0.5Ωcm.

Figs. 5(a) and 5(c) show that the loss by SRH recombination in cell 290-1.5 is 17% lower than in cell 290-0.5. The reason for this is a higher diffusion length and a lower quasi-Fermi level splitting in 290-1.5. Both cell groups, however, are not limited by this loss mechanism. The emitter recombination is the only loss mechanism which decreases with decreasing base resistivity. The electrical shading affects a larger part of the cell at a lower base resistivity (0.5Ωcm) than at a higher base resistivity (1.5Ωcm), as illustrated in Fig. 5.

All these effects lead to the conclusion

that a base resistivity of 1.5Ωcm should be used instead of 0.5Ωcm, since the former results in decreased power losses by Auger, SRH and rear-surface recombination for a thickness of 290µm and a high base lifetime of 3000µs to 4000µs.

"A base resistivity of 1.5Ωcm should be used instead of 0.5Ωcm, since the former results in decreased power losses by Auger, SRH and rear-surface recombination."

Simulating the optimum conversion efficiency dependent on cell thickness, base doping and base lifetime

In order to evaluate a larger parameter space, a simulation study was carried out to analyze the impact on the solar cell conversion efficiency of base doping combined with cell thickness for different base lifetimes. The simulations are based on the same measured geometries and recombination parameters as those obtained for the experimental cells. Figs. 6 and 7 are valid for different base lifetimes of 20µs (measured on the epitaxial layer cell) and 3000µs (measured on the float-zone wafer cell). Both Figures show the solar cell conversion efficiency for doping densities of 10^{14}cm^{-3} to 10^{17}cm^{-3} and cell thicknesses of 18µm to 290µm. The arrows indicate how the different loss mechanisms influence the conversion efficiency.

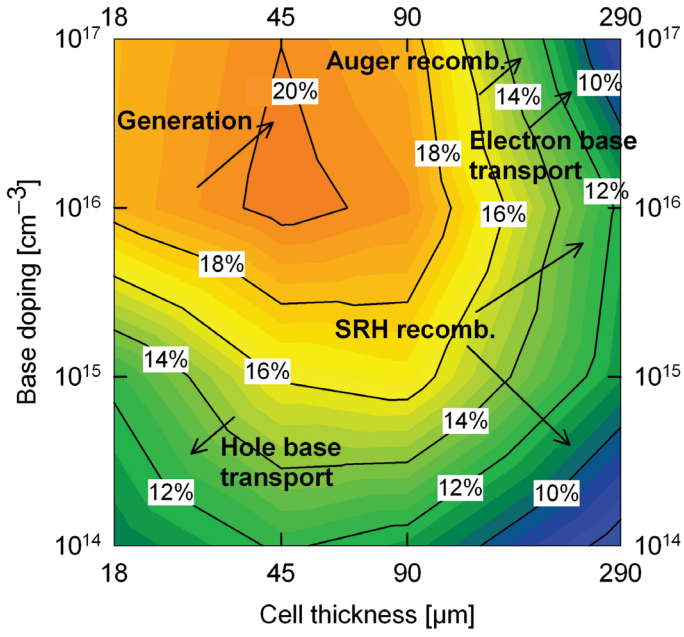

Figure 6. Solar cell conversion efficiency as a function of the base doping and cell thickness for a base lifetime of 20µs. The impact of the free energy of generation as well as loss mechanisms is indicated by arrows. (Adapted from Haase et al. [19].)

Fig. 6 shows the efficiency for a minority-carrier lifetime of 20µs. The efficiency decreases with decreasing cell thickness (lower generated free energy) and decreasing base doping. Resistive losses by majority carriers in the lateral direction also increase with decreasing cell thickness owing to an increased sheet resistance in the base. The sheet resistance also increases with decreasing base-doping concentration, which in turn decreases the conversion efficiency.

On the other hand, the transport of electrons increases with increasing cell thickness and base doping. The minority-carrier concentration increases with increasing cell thickness. This increase in carrier concentration increases SRH recombination, which decreases the efficiency. Auger recombination also increases with increasing cell thickness because of the quasi-Fermi level gradient to the front surface, which also decreases the efficiency. Auger recombination also increases quadratically with increasing base doping. For a base lifetime of 20µs, these are the main effects that lead to a maximum efficiency at a cell thickness of 45µm and a base-doping density between 10^{16}cm^{-3} and 10^{17}cm^{-3}.

Fig. 7 shows the efficiency for a minority carrier lifetime of 3000µs. For this lifetime the effect of SRH recombination is reduced compared to the 20µs lifetime, and the diffusion length does not significantly limit efficiency in the case of cell thicknesses up to 290µm. The efficiency presents a maximum for a base-doping concentration of about 10^{16}cm^{-3}. The limiting parameters for thin cells with a lifetime of 3000µs are the decreased generation and the base resistance losses. The maximum efficiency is greater than 23% for cell thicknesses above 290µm, but if the thickness is reduced from 290µm to about 90µm, the power loss is less than 0.6% absolute. The generation may be enhanced by improved light trapping, whereas the base resistance losses may be reduced by a highly doped

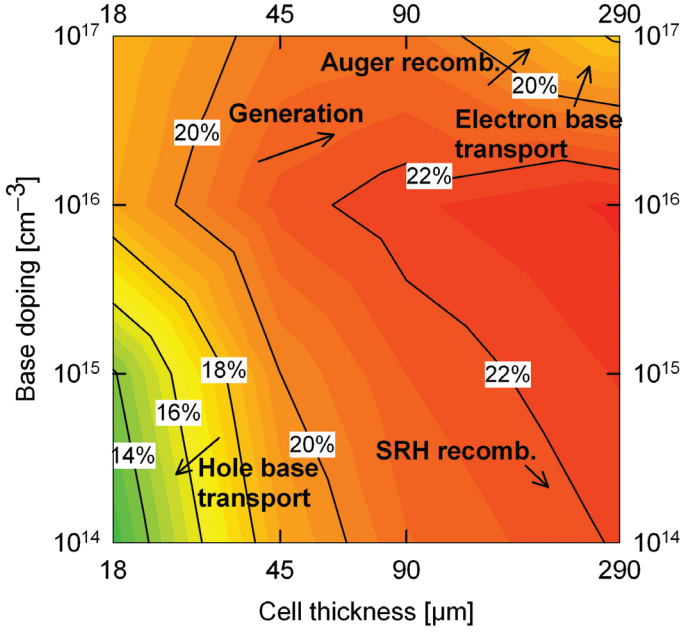

Figure 7. Solar cell conversion efficiency as a function of the base doping and cell thickness for a base lifetime of 3000µs. The impact of the free energy of generation as well as loss mechanisms is indicated by arrows. (Adapted from Haase et al. [19].)

7th PV Fab Managers Forum

Roadmap to manufacturing excellence and greater productivity in a challenging business environment.

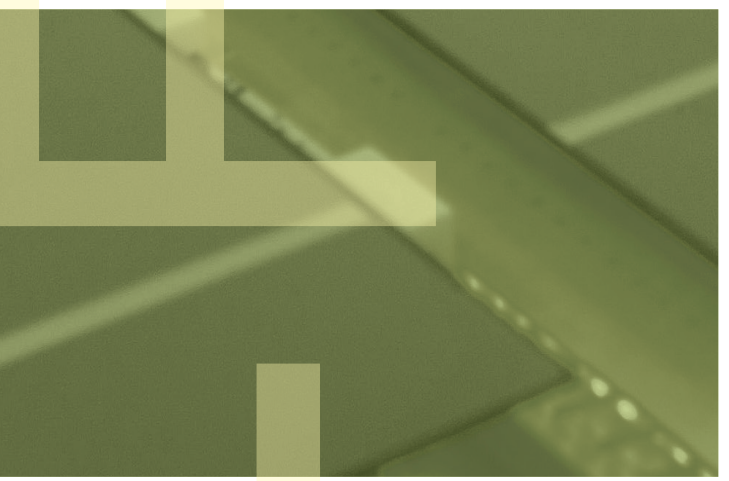

www.pvgroup.org/pvfmf

Forum Topics:

- PV Market and Manufacturing Technology Outlook
- International Technology Roadmap for PV (ITRPV)
- Cost Reduction Potentials in Cell and Module Manufacturing
- Efficiency Increase Potentials in Cell and Module Manufacturing
- PV Standardization Update and Overview

Sponsored by: DAS Environmental Expert.

Industry supporters:

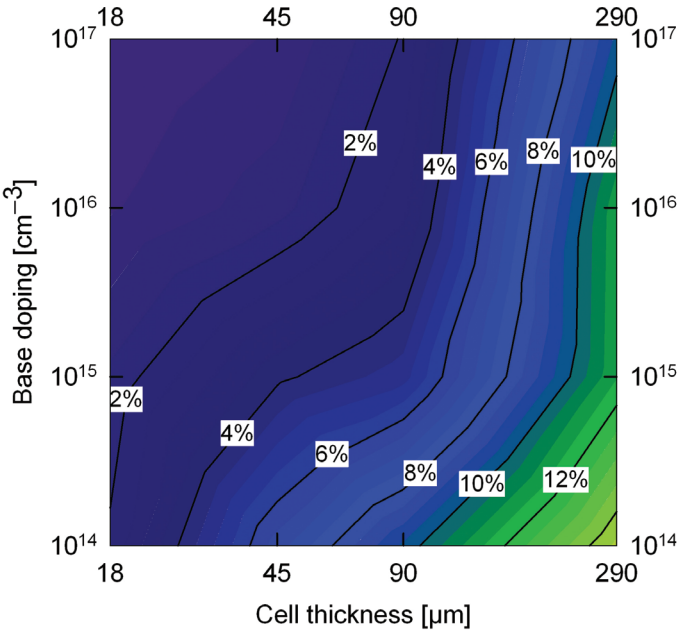

Figure 8. Difference between solar cell conversion efficiencies for base lifetimes of 3000µs and 20µs as a function of base doping and cell thickness.

layer (e.g. at the front surface), which deceases the base sheet resistance but does not significantly increase the recombination. Another possibility for reducing the resistance losses is to shorten the current path lengths by changing the geometry of the cell (e.g. smaller unit cells).

Fig. 8 shows the difference between solar cell conversion efficiencies for base lifetimes of 3000µs and 20µs. The difference in conversion efficiency is less than 1% absolute at doping densities of more than 10^{16}cm^{-3} and cell thicknesses of less than 45µm. At lower doping densities and higher cell thicknesses, the difference in efficiency increases to more than 14% absolute, which is mainly due to the increase in SRH recombination.

> "The highest efficiency of 22.6% was measured on a 130µm-thick, 1.5Ωcm-resistivity cell with a base lifetime of 4000µs."

Conclusion

The fabrication and analysis of high-efficiency BJBC cells has been demonstrated. The highest efficiency of 22.6% was measured on a 130µm-thick, 1.5Ωcm-resistivity cell with a base lifetime of 4000µs. A 290µm-thick cell with a resistivity of 1.5Ωcm showed almost the same efficiency (22.5%), since an increase in generation offsets any increase in front and base recombination. The simulation study, which is based on measured input parameters, showed the impact of the loss mechanisms on the conversion efficiency. The maximum efficiency shifts to a larger cell thickness, with increasing base lifetime for a BJBC cell. The maximum efficiency for a BJBC is around 10^{16}cm^{-3} base-doping density, since Auger recombination and transport losses by electrons increase with higher base-doping density, and lateral transport losses by holes increase with lower base-doping density. BJBC cells with cell thicknesses of about 45µm allow a reduced material consumption combined with a high conversion efficiency of about 21%, assuming a base lifetime of 3000µs, which is only reduced by about 1% absolute if the base lifetime is reduced to 20µs. BJBC cells with base lifetimes of 3000µs show an efficiency of more than 23% for cell thicknesses greater than 290µm; this is only reduced by 0.6% absolute if the cell thickness is reduced from 290µm to 90µm.

Acknowledgements

The authors express their gratitude to J. Hensen for the electrochemical etching, J. Käsewieter for assistance at the lift-off stages, T. Neubert for support in the laser processes, A. Merkle for valuable advice during the processes, and the Renewable Energy Corporation ASA for funding this work.

References

[1] Cousins, P.J. et al. 2010, "Generation 3: Improved performance at lower cost", *Proc. 35th IEEE PVSC*, Honolulu, Hawaii, USA, pp. 275–278.

[2] Gee, J.M. et al. 1997, "Simplified module assembly using back-contact silicon solar cells", *Proc. 26th IEEE PVSC*, Anaheim, California, USA, pp. 1085–1088

[3] Köntges, M. et al. 2008, "A novel photovoltaic-module assembly system for back contact solar cells using laser soldering technique", *Proc. 23rd EU PVSEC*, Valencia, Spain, pp. 2709–2712.

[4] de Jong, P.C. et al. 2004, "Single-step lamination full-size PV module made with back-contact mc-Si cells and conductive adhesives," *Proc. 19th EU PVSEC*, Paris, France, pp. 2145–2148.

[5] Mo, C.B. et al. 2012, "High efficiency back contact solar cell via ion implantation", *Proc. 27th EU PVSEC*, Frankfurt, Germany [in press].

[6] Grohe, A. et al. 2012, "High-efficient ion implanted back contact cells for industrial application", *Proc. 27th EU PVSEC*, Frankfurt, Germany [in press].

[7] Schneiderlöchner, E. et al. 2002, "Laser-fired rear contacts for crystalline silicon solar cells", *Prog. Photovolt.: Res. Appl.*, Vol. 10, No. 1, pp. 29–34.

[8] Chih-Tang, S. et al. 1982, "Effect of thickness on silicon solar cell efficiency", *IEEE Trans. Electron. Dev.*, Vol. 29, No. 5, pp. 903–908.

[9] Kray, D. & McIntosh, K.R. 2009, "Analysis of ultrathin high-efficiency silicon solar cells", *physica status solidi A*, Vol. 206, pp. 1647–1654.

[10] Tayanaka, H. et al. 1998, "Thin-film crystalline silicon solar cells obtained by separation of a porous silicon sacrificial layer", *Proc. 2nd WCPEC*, Ispra, Italy, p. 1272.

[11] Brendel, R. et al. 1997, "A novel process for ultrathin monocrystalline silicon solar cells on glass", *Proc. 14th EU PVSEC*, Barcelona, Spain, p. 1354.

[12] Dross, F. et al. 2008, "Slim-cut: A kerf-loss-free method for wafering 50-µm-thick crystalline Si wafers based on stress-induced lift-off", *Proc. 23rd EU PVSEC*, Valencia, Spain, pp. 1278–1281.

[13] Henley, F. et al 2008, "Direct film transfer (DFT) technology for kerf-free silicon wafering", *Proc. 23rd EU PVSEC*, Valencia, Spain, pp. 1090–1093.

[14] AstroWatt [details online at http://www.astrowatt.com].

[15] Petermann, J.H. et al. 2012, "19%-efficient and 43µm-thick crystalline Si solar cell from layer transfer using porous silicon", *Prog. Photovolt.: Res. Appl.*, Vol. 20, pp. 1–5.

[16] Horbelt, R. et al. 2005, "Demonstration of the manifold use of growth substrates in the porous silicon process", *Proc. 31st IEEE PVSC*, Orlando, Florida, USA, pp. 1193–1196.

[17] Steckenreiter, V. et al. [in preparation].
[18] Engelhart, P. et al. 2006, "Laser-ablation of passivating SiN_x layers for locally contacting emitters of high-efficiency solar cells", *Proc. 4th WCPEC*, Waikoloa, Hawaii, USA, p. 1024.
[19] Haase, F. et al. 2012, "High efficiency back-contact back-junction silicon solar cells with cell thicknesses of 45 µm, 90 µm, 130 µm and 290 µm", *Proc. 27th EU PVSEC*, Frankfurt, Germany [in press].
[20] Sinton, R.A. et al. 1988, "Development efforts in silicon backside-contact solar cells", *Proc. 8th EU PVSEC*, Florence, Italy, p. 472.
[21] Brendel, R. 1994, "Sunrays: A versatile ray tracing program for the photovoltaic community", *Proc. 12th EU PVSC*, Amsterdam, Netherlands, pp. 1339–1342.
[22] Kane, D.E. & Swanson, R.M. 1985, "Measurement of the emitter saturation current by a contactless photoconductivity decay method", *Proc. 18th IEEE PVSC*, Las Vegas, Nevada, USA, p. 578.
[23] Ramspeck, K. et al. 2009, "Dynamic ILM – an approach to infrared-camera-based dynamical lifetime imaging", *Proc. 24th EU PVSEC*, Hamburg, Germany, pp. 871–876.
[24] Haase, F. et al. 2011, "Loss analysis of back-contact back-junction thin-film monocrystalline silicon solar cells", *J. Appl. Phys.*, Vol. 110, p. 124510.
[25] Yablonovitch, E. et al. 1986, "Unusually low surface-recombination velocity on silicon on germanium surfaces", *Phys. Rev. Lett.*, Vol. 57, p. 249.
[26] Brendel, R. 2012, "Modeling solar cells with the dopant-diffused layers treated as conductive boundaries", *Prog. Photovolt.: Res. Appl.*, Vol. 20, pp. 31–43.
[27] COMSOL Multiphysics 3.5 [details online at http://www.comsol.com/products/3.5].
[28] Brendel, R. et al. 2008, "Theory of analyzing free energy losses in solar cells", *Appl. Phys. Lett.*, Vol. 93, No. 17, p. 173503.
[29] Hermle, M. et al. 2008, "Shading effects in back-junction back-contacted silicon solar cells", *Proc. 33rd IEEE PVSC*, San Diego, California, USA, pp. 1064–1068.

About the Authors

Felix Haase received a physics diploma degree, with a focus on absorbers for thin-film silicon solar cells by fluid phase processing, from the Friedrich-Alexander-Universität Erlangen-Nürnberg in 2007. Since then he has been a Ph.D. candidate at the Institute for Solar Energy Research Hamelin (ISFH). His work involves developing and characterizing BJBC thin-film monocrystalline silicon solar cells processed by the porous silicon process (PSI).

Sarah Kajari-Schröder received a diploma degree in physics in 2004, for which she focused on theoretical quantum optics, and then a Ph.D. degree in 2009 for her research on the Hamiltonian ratchet effect, both from the University of Ulm in Germany. She then joined the PV module group of ISFH, where her research involved crack formation in solar cells, and mechanical stability and reliability of photovoltaic modules. Since 2011 she has been head of the silicon thin-film research group at ISFH, where she concentrates on the fabrication, handling and interconnection of ultrathin crystalline silicon wafers and solar cells.

Renate Winter joined ISFH in 2008 and specializes in the processing of ultrathin monocrystalline silicon solar cells. After completing her professional training as a mechanical technological textile laboratory technician, she worked for 28 years for the carpet manufacturer Besmer GmbH.

Martin Nese received his M.Sc. degree in applied physics in 1989 from the Norwegian University of Science and Technology, with a thesis on photoluminescence spectroscopy of III-V materials. In 1990 he became a scientist at SINTEF within the field of silicon MEMS and silicon radiation detection technologies, after which, in 1996, he became a project manager at SensoNor, specializing in silicon MEMS sensors for automotive applications. He then joined Presens in 1997 as CTO for high-precision sensors. In 2007 he became a technology manager at REC, overseeing the strategic development of future PV technology platforms, and co-founded EPISUN in October 2012, aiming to develop and industrialize future PV technology platforms based on ultrathin silicon wafers and novel module interconnection methods.

Rolf Brendel is the scientific director of ISFH. He received his Ph.D. in materials science from the University of Erlangen, Germany, for his work on infrared spectroscopy. In 2004 he joined the Institute of Solid State Physics at the Leibniz University of Hanover as a full professor. His main research focuses on the physics and technology of crystalline silicon solar cells.

Enquiries

Felix Haase
Institute for Solar Energy Research Hamelin (ISFH)
Am Ohrberg 1
D-31860 Emmerthal
Germany
Phone: +49-5151-999-313
Fax: +49-5151-999-400
Email: f.haase@isfh.de